Available online at www.sciencedirect.com
ScienceDirect
Journal of Power Sources 167 (2007) 366–377
JOURNAL OF POWER SOURCES
www.elsevier.com/locate/jpowsour

On mechanical behavior and in-plane modeling of constrained PEM fuel cell membranes subjected to hydration and temperature cycles

Roham Solasi [a,*], Yue Zou [a], Xinyu Huang [a], Kenneth Reifsnider [a], David Condit [b]

[a] *Connecticut Global Fuel Cell Center, University of Connecticut, Storrs, CT 06269, USA*
[b] *United Technologies Research Center, East Hartford, CT 06108, USA*

Received 25 January 2007; accepted 7 February 2007
Available online 22 February 2007

Abstract

Currently, ionomer membranes are used in a variety of specialized applications. Such applications include, but are not limited to, dialysis, electrolysis, membrane separators, reaction catalysts and the most promising application: polymer electrolyte fuel cells. Although their use is widespread, significant gaps in understanding the mechanical behavior of these materials still remain. Many ionomer membranes change their structure, and in turn, their mechanical properties in response to applied thermal and moisture conditions that are functions of position. It has been observed that constrained materials subjected to changing environmental conditions can exhibit unusual behavior, e.g., in some cases, mechanical failure is seen in the absence of external applied mechanical loads. This condition is especially important in polymer membranes (specifically Nafion®) used in polymer electrolyte membrane (PEM) fuel cells and is the major motivation of the present work. Laboratory characterization has been conducted to determine the mechanical properties of a proton exchange membrane with respect to temperature and relative humidity. Data recovered in these tests along with properties from literature have been used in finite element models to predict the behavior of membranes used in certain applications and geometries. The overall goal of this investigation was to characterize the mechanical response of ionomer membranes in in-plane constraint configurations subjected to variable hygro-thermal environments. Expansion/contraction mechanical response of the constrained membrane as a result of change in hydration and temperature is studied in uniform and non-uniform geometries and environments. With this information, mechanical failure modes can be analyzed which is necessary for durability modeling and life prediction. The present work concentrates on defining and understanding the basic mechanical behavior of ionomeric membranes clamped in a rigid frame, and subjected to changes in temperature and humidification.

Keywords: Ionomer; Polymer electrolyte membrane (PEM); Mechanical response; Hygro-thermal; Nafion®; Constraint

1. Introduction

Polymer electrolyte membrane (PEM) fuel cells, which utilize hydrogen to generate electricity through electrochemical reactions, may be an environmental-friendly replacement for current internal combustion engines in transportation (and other) applications. Durability and cost are the major barriers to the commercialization of PEM fuel cells. The DOE durability and cost targets (2015) set for an 80 kW (net) transportation fuel cell stack (excluding balance of plant BOP) are a lifetime of 5000 h over a wide range of temperature and a per-kilowatt cost of 15 dollars or less (which corresponds to 20 dollars per square meter for polymer electrolyte membranes) [1]. Membrane failure is one of the major stack life-limiting factors, which reduces the durability to the current 2000 h status (2006). To meet the DOE durability targets, fundamental understanding of the degradation and mechanical failure of ionomer membranes in the PEMFC stacks is necessary to help mitigate this type of failure. In order to establish a mechanistic durability and life prediction model, three steps have to be taken: (1) investigate the mechanical behavior of ionomer membrane; (2) establish accurate numerical stress–strain constitutive modeling methods for PEMFC stacks; (3) identify material's degradation and failure mechanisms and kinetics for use in a mechanistic-based life prediction model.

* Corresponding author. Tel.: +1 860 748 6188; fax: +1 860 486 8378.
E-mail addresses: roham@engr.uconn.edu (R. Solasi), yue@engr.uconn.edu (Y. Zou), xinyu@engr.uconn.edu (X. Huang), reifsnider@engr.uconn.edu (K. Reifsnider), conditda@utrc.utc.com (D. Condit).

0378-7753/$ – see front matter © 2007 Elsevier B.V. All rights reserved.
doi:10.1016/j.jpowsour.2007.02.025

This work will focus on the second part in conjunction with the previous investigations performed by the authors to tackle the outlined steps.

The most commonly used membrane in PEM fuel cells is a perfluorosulfonic acid (PFSA) membrane. Among the PFSA polymers used in fuel cells the most favored one has been the sulfonated tetrafluoroethylene copolymer with the trade name Nafion®, developed and manufactured by DuPont™ in the 1960s. It is the first of a class of synthetic polymers with ionic properties, which are called ionomers [2]. Nafion® has a very complex structure which has intrigued scientists for decades especially in the recent years when new applications in fuel cells appeared to be a solution to energy problems. Although there are a variety of models to describe Nafion®'s structure, it is still not very clear how it changes in different environments. Nafion® consists of a hydrophobic polytetrafluoroethylene (PTFE)-like backbone and pendent chains with sulfonated (SO_3^-) end groups. Under humidified conditions, the hydrophilic end groups segregate into nano-sized clusters, which imbibe water and cause the swelling of the ionomer. The phase-separated morphology and the ionic conducting mechanisms of Nafion® have been extensively studied and more research is underway to understand the micro/nano behavior of perfluorosulphonated ionomers [3–15]. These water clusters form interconnected acidic domains, which are also thought to be the major path for proton transport. Both the swelling and the proton conductivity increase with the level of hydration [16–20]. The mechanical behavior of Nafion® is also known to be a strong function of hydration [21–26].

Membrane failure is believed to be the result of combined chemical and mechanical effects acting together [27,28]. Variations in temperature and humidity during operation cause cyclic stresses and strains (mechanical loading) in the membrane as well as the MEA and is considered to be the mechanical failure driving force in fuel cell applications [21,29–31]. Reactant gas cross over, hydrogen peroxide formation and movement, and cationic contaminants are all believed to be major factors contributing to the chemical decomposition of polymer electrolyte membranes. Huang et al. have observed localized attack of Nafion® under open circuit voltage (OCV) degradation leading to crossover failure. This localized membrane attack begins on the cathode-side and is rapid in dry and hot conditions [28]. When exacerbated by mechanical effects, e.g., relative humidity cycling, it leads quickly to crossover failure as numerous pores/cracks propagate across the MEA and pinholes will be formed [20,27,32,33]. These pinholes cause gas crossover and localized heating of the membrane and can eventually lead to catastrophic failure of the fuel cell stacks.

While chemical degradation of prefluorinated membranes has been investigated and reported extensively in literature [34–43], there has been little work published on mechanical degradation of the membrane. Cyclic hydration of the membrane/MEA during the operation cycles (start/shut down) of the fuel cell and hence mechanical fatigue of the membrane electrode assembly has been shown to cause mechanical degradation of the membrane [29]. Investigating the mechanical response of the membrane subjected to fuel cell cycles requires studying and modeling of the stress–strain behavior of membranes and MEAs. Weber and Newman were the first to study the stress associated with constraint in a simple one-dimensional model [44]. A finite element model has been used by Tang et al. to investigate the hygro-thermal stresses in a cell assembly caused by temperature and relative humidity change with an assumption of linear elastic behavior for the membrane [31,45]. Later, Kusoglu et al. modified the work to simulate the stress evolution during a simplified operating cycle using a linear elastic-perfectly plastic material model. They have shown that compressive, plastic deformation occurs during the hygro-thermal loading, resulting in tensile residual stresses after unloading [30].

It has been shown that stress relaxation of Nafion® is highly influenced by introducing water in the structure; thus, any visco-elastic/plastic model for Nafion® should consider hydration effects in the stress model [46]. Benziger and Chia proposed that membrane swelling and relaxation processes work as an interfacial contact switch between the membrane and the catalyst layer. In this case stress relaxation causes the extruded membrane into the electrode to slowly relax and stretch out in the plane of membrane [47]. The importance of the relaxation and also the existing time delays during hydration/dehydration of the membrane in fuel cells reveals the significance of adding viscous contribution to the stress model. A visco-elastic stress model has been developed by Lai et al. and stress predictions upon implementing the model using the data for Nafion® NR111 have been validated with stress measurements from a relaxation test performed at small initial strain (3%) in the linear elastic region. They have also treated Nafion® as a rheologically simple material and applied time–temperature–moisture superposition principles to generate master curves for creep compliance of Nafion® [29]. In the authors' previous studies, the properties obtained for a wide range of temperature and hydrations have been applied in a finite element model to study through-thickness stress–strain behavior of an MEA as a result of hydration and temperature cycling during MEA fabrication and/or unitization with GDLs. Geometric irregularities have been introduced to induce high local stress–strain concentrations, and as potential sources for crazing and crack-like defects leading to final mechanical failure of the MEA [21]. The same elastic–plastic material model has also been used for in-plane numerical modeling of RH-induced strain in an MEA in a constraint configuration [28]. In the present paper, a two-layer visco-plastic model is proposed to predict strain rate dependence and relaxation behavior of a membrane, and will also be discussed further in a future work.

This paper focuses on a mechanical modeling scheme of the membrane in order to simulate the stress–strain response of the membrane in the constrained frame. This in-plane constraint configuration roughly mimics the clamped membrane in the fuel cell. Changes in hydration and temperature will be the driving forces, and hydration will be shown to have a bigger effect. It is important to understand that without any external applied force, the membrane can be weakened primarily by chemical reactions and by cyclic hydration, and can subsequently fail mechanically in the constrained geometry. Thus, hydration (and to lesser extent temperature) acts as the driving force for mechanical breach and formation of pinhole/cracks

in the framed membrane. This article is outlined as follows. Mechanical properties of Nafion® are presented as a function of relative humidity and temperature. Then those material curves have been incorporated into the commercial finite element code ABAQUS (HKS). Coefficients of hydration expansion as the most important physical parameters are determined from literature data [19]. Strains induced by the hydration change are validated using a three-sided constrained membrane in a frame. Based on the obtained material properties simulations have been run for a four-sided clamped membrane exposed to hydration and temperature cycles. Stress–strain results are also compared for a clamped membrane with a center hole and results are shown for 10 hydration and temperature cycles. In the last section of the paper, the time (strain-rate) dependent visco-plastic behavior of the membrane is introduced and discussed.

2. Material properties as a function of T and RH for ionomer membrane (Nafion® 111)

Mechanical properties of Nafion® (in this study commercial Nafion® NR111 has been used) are strong functions of relative humidity (water uptake) and temperature. Thus, in order to accurately characterize Nafion®'s properties it is critical to study its mechanical behavior for different environments. Uniaxial tensile testing was used to investigate the material mechanical properties as a function of T and RH. Tests were carried out in an environmental chamber (gas chamber) with independent RH and T control, built on an MTS Tytron machine. A water bath tray was also designed to enable tensile testing with the membrane sample fully immersed in water. The specimen was cut into rectangular shape with about 50 mm length and 6.5 mm width. The width of membrane sample was measured at three different locations across the length of the specimen before the test in room condition. All tests were performed at a constant strain rate of approximately $0.014\,s^{-1}$, but slight changes in strain rate did not show significant influence on mechanical properties of the material. The original cross-sectional area and gauge length of the specimens were used in calculating the stress–strain curves from the displacement–load data.

Fig. 1 shows the engineering stress–strain curves of as-received Nafion® NR111 membrane at 25 °C with different RH from dry to wet (fully immersed in liquid water). Typical stress–strain curves of the membrane in water vapor environment have a "bilinear" shape consisting of a linear elastic region and a linear plastic region, which are interconnected by the yielding region, while typical stress–strain curves of membranes immersed in liquid water appear to have a power law shape with no distinct yield region. The elastic modulus was obtained by calculating the initial slope of the stress–strain curve. The yield point was defined to be the intersection of extended linear parts of the elastic and plastic region. This behavior transition is believed to be the result of internal structural change due to water uptake. With the increase in water content, there is a decrease of both elastic modulus and yield stress. The slope of the plastic region (secondary slope) also seems to decrease with increasing RH. Water, absorbed by polymer, has been recognized as a plasticizer, which will soften the material and reduce the load

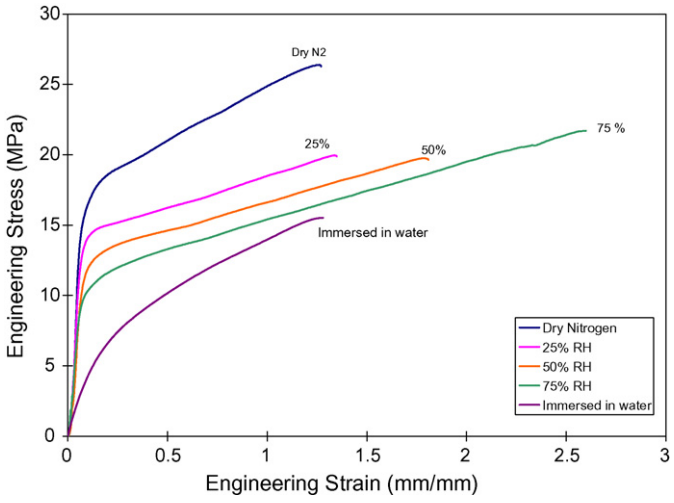

Fig. 1. Stress–strain curves of Nafion® NR111 membrane in 25 °C with varying RH.

carrying capability [48]. Stress–strain curves of the membrane in 50% RH with different temperatures from 25 °C to 80 °C are presented in Fig. 2. It can be seen that the elastic modulus and yield stress are decreasing with increasing temperature. Temperature seems to have a more significant effect on mechanical properties of Nafion® membrane than hydration, especially on the yield stress. Slight change in the secondary slope is also observed when T varies. However, comparing to elastic modulus and yield stress, the influence of T and RH on the secondary slope is less significant.

Poisson's ratio was obtained experimentally by using a video extensometer and tracing the forward and lateral displacement of pre-drawn dots on the membrane during the uniaxial test. It should be mentioned that Poisson's ratio could also be a function of hydration and temperature as well. While this issue will be addressed in another paper, initial results of our experiments have shown that this dependence is not significant and therefore it has been assumed to be a constant equal to 0.4 in the present work.

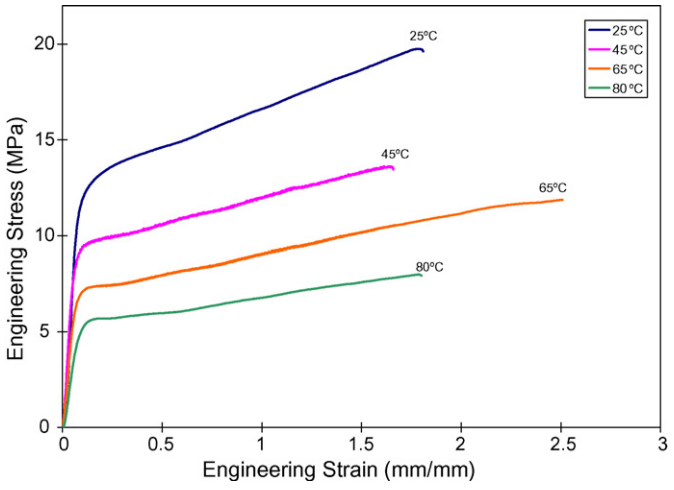

Fig. 2. Stress–strain curves of Nafion® NR111 membrane in 50% relative humidity and various temperatures.

3. Incorporation of the material model into FEM

In PEM fuel cells, the membrane (as part of the membrane electrode assembly) is clamped on four edges. This kind of in-plane geometry will be addressed in this paper and out-of-plane pressure will be ignored. Clamped boundary conditions can be the clamped seal regions or the local clamps applied by ribs of bipolar plates (flow fields) on the membrane. Therefore, ignoring the out-of-plane forces does not affect the generality of the model. It is important to point out that there is no external applied mechanical force and that changes in hydration and temperature are the only driving forces in this simulation. In order to calculate accurate numbers for hydration and temperature induced strains it is needed to define the coefficients of hydration and temperature expansion referred to as α and β in this paper. Having proper numbers for alpha and beta, correct values for hygro-thermal stresses, which are the major mechanical forces in the model, will be calculated by a finite element code according to the following expressions in matrix notation [49]:

$$\{\sigma\} = [S]^{-1}(\{\varepsilon\} - \{\alpha\}\Delta T - \{\beta\}\Delta\lambda) \quad (1)$$

where $\{\sigma\}$ and $\{\varepsilon\}$ are mechanical stress and strain tensors due to change in hydration and temperature and $[S]$ is the material compliance matrix. α and β are the coefficients of thermal and hydration expansion and ΔT and $\Delta\lambda$ are changes in temperature and hydration, respectively. Note that if material is unrestrained during the hygro-thermal exposure, there are no stresses generated and the strains are given by

$$\{\varepsilon\} = \{\varepsilon_{hg}\} = \{\alpha\}\Delta T + \{\beta\}\Delta\lambda \quad (2)$$

If the material is completely restrained during hygro-thermal exposure, however, the total strain must be zero. Thus,

$$\{\varepsilon\} = 0 = [S]\{\sigma\} + \{\alpha\}\Delta T + \{\beta\}\Delta\lambda \quad (3)$$

and the resulting hygro-thermal stresses are given by:

$$\{\sigma\} = [S]^{-1}(-\{\alpha\}\Delta T - \{\beta\}\Delta\lambda) \quad (4)$$

Establishing the proper value for the coefficient of hydration expansion (β) is a key component in the finite element model. Nafion® expands/shrinks to a great extent when exposed to hydration cycles. Shrink tension and membrane expansion induce stress cycles in the membrane during fuel cell operation. Changes in dimension with hydration are orders of magnitude bigger than we would expect from changes in temperature. In the fuel cell this change in hydration (relative humidity) is equivalent to mechanical load and is believed to be a major driving force for mechanical failure. Numbers for coefficients of hydration expansion for Nafion® have been extracted from the graphs presented by Morris and Sun [19] as shown in Fig. 3. They have obtained two curves for change in diameter and thickness of membranes. Assuming these two curves are linear, slopes of the two lines will be the βs along the diameter and thickness in the model, β_x and β_y. These two values are 0.013 and 0.008, respectively, and have been incorporated into the model – along with coefficients of thermal expansion α – by the ABAQUS user subroutine UEXPAN [50]. For all the in-plane simulations presented in this paper just the first value is used.

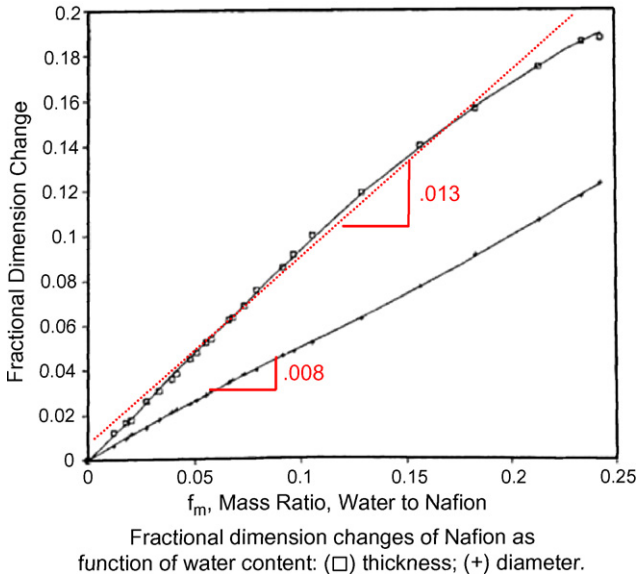

Fig. 3. Coefficients of hydration expansion along the diameter and thickness of Nafion®. *X*-axis is mass ratio of water to Nafion® f_m, while *Y* axis is dimensional change. Water content of membrane (λ) is equal to $61.0 \times f_m$ [19].

Material properties (uniaxial stress–strain curves) for the Nafion® as shown in the previous section are obtained as a function of temperature and relative humidity. Hence, water content, as an independent field variable in finite element modeling, must be related to relative humidity for different temperatures. Springer et al. found a relationship between water content and relative humidity of Nafion® [51]. This equation (Eq. (5)) relates relative humidity (water vapor activity) to water uptake from water vapor at room temperature (30 °C).

There is controversy in the literature on the relationship between Nafion®'s water content and relative humidity with change in temperature. Some researchers found that for a certain relative humidity, water uptake decreases when temperature increases [18,52–54] while others reported the opposite trend in which water uptake goes up as temperature rises [19,55,56]. Hinatsu et al. reported the relationship for different temperatures pointing out that the shape is similar for all the temperatures [18]. Eq. (6) is the equation they derived for $T = 80$ °C which shows that water content at 80 °C is less than that reported for the lower temperatures. They have related this temperature effect to difficulty in condensing water on the membrane surfaces at higher temperatures. Eqs. (5) and (6) will be used in this paper to relate λ (water content) to relative humidity (water activity).

$$@T = 25\,^{\circ}\text{C} : \lambda = 0.043 + 17.81a - 39.85a^2 + 36.0a^3 \quad (5)$$

$$@T = 80\,^{\circ}\text{C} : \lambda = 0.300 + 10.8a - 16.0a^2 + 14.1a^3 \quad (6)$$

Values for other temperatures can be interpolated (extrapolated) from these two equations. The value of the coefficient of thermal expansion (α) is chosen to be 1.47×10^{-4} [57].

These equations have been obtained for membranes in contact with water vapor, which is the primary water uptake mechanism for fuel cell humidification. Water uptake from the liquid phase

with unit water activity (100% relative humidity) is higher than water uptake from the saturated vapor phase, a phenomenon known as Schroeder's paradox [58]. This phenomenon is the main reason why water content is used as a field variable instead of relative humidity in the numerical simulations. This prevents ambiguities when it comes to fully saturated environments (RH = 100%, vapor or liquid phase) and numerical convergence problems with associated computations are unlikely to happen for that reason. For instance, for unit water activity at room temperature, the water content in the membrane can be any number from 14 to 22; this imposes different swelling conditions and therefore different stress states in the membrane, which is hard to represent in the numerical code. It has been reported in literature that unlike the case of water uptake from the vapor phase, water uptake in the liquid phase goes up with increasing temperature. Membranes placed in water at 100 °C for 1 h absorbed almost twice the amount of water as membranes placed in water at 25 °C for 24 h [24]. This issue must be addressed in water electrolyzers where the membrane is in contact with liquid water, but will not be considered here. Physically, a membrane sandwiched between two bipolar plates has a lower value of λ compared to a free swollen one that is not constrained. Pressure from bipolar plates in a fuel cell configuration can push some water out of the membrane in a similar way as a squeezed sponge [44,47]. This effect has not been accounted for in the presented simulations.

In order to model the strains/stresses developed during the RH and temperature cycling of a clamped membrane, hydration-dependent changes of material properties during RH (and T) variation have been incorporated into the commercial finite element (FE) code ABAQUS (HKS). The measured T and RH (or λ) dependent stress–strain responses discussed in the previous section of this paper were incorporated into the simulation model through the ABAQUS built-in elasto-plastic material model. The λ-dependent material properties were implemented through look up tables, such as:

*ELASTIC	*PLASTIC
$E_1, \nu_1, T_1, \lambda_1$	$\sigma_1, \varepsilon_{p1}, T_1, \lambda_1$
$E_2, \nu_2, T_2, \lambda_2$	$\sigma_2, \varepsilon_{p2}, T_2, \lambda_2$
...	...

where E and $\nu = 0.4$ are the elastic modulus and Poisson's ratio, respectively; σ and ε_p are true stress and strain extracted from the plastic region of the stress–strain curve; T and λ are the corresponding temperature and water content (RH). The following equations are used to convert engineering stress–strain to the true stress–strain values needed in FEA.

$$\varepsilon_{true} = \ln(1 + \varepsilon_{engr}) \quad (7)$$

$$\sigma_{true} = \sigma_{engr}\, e^{2\nu \ln(1+\varepsilon_{engr})} \quad (8)$$

As the applied RH changes, ABAQUS updates the materials constitutive behavior according to the table. There is no external mechanical force applied in the simulation of the clamped membrane and the only driving force is the change in hydration as an independent field variable. It can be easily concluded from the values of α and β and Eqs. (1) and (2) that hydration has a far bigger effect than temperature on shrinkage/expansion of membranes in the fuel cell environment. For this reason, change in hydration will be the primary driving force in all the present simulations. At the same time, change in temperature will also be applied in order to pick the appropriate material curves during the simulation. It is also known that Nafion®, as a polymer, demonstrates time-dependent behavior such as creep and stress relaxation. That behavior was not incorporated in this reported model, but it can be included in the model and will be discussed in a future work by adding a viscous module to this elasto-plastic model.

4. Validation of strains and hydration coefficients

In the experiment conducted to verify the FEM results, a rectangular fully hydrated specimen was clamped in a rigid frame. A 26 mm × 23 mm specimen of NR111 was used. Three edges of the specimen were constrained and black dots have been made on one edge of the specimen to be traced by the video-extensometer. After waiting for the dots to dry, the specimen was hot pressed at 100 °C to ensure the dots adhered to the membrane. The membrane was then boiled in DI water for about an hour. It was then placed in the designed frame such that three of the membrane edges were constrained and the dotted edge remained free. During installation of the specimen on the frame, two pieces of wet Kimwipe™ were placed on both sides of the membrane to reduce water loss during mounting. After tightening the bolts of the frame the Kimwipes™ were removed and extra water on the surface of membrane and also on the frame was blotted with Kimwipe™. The front surface of the clamped membrane was viewed by a video-extensometer to trace the displacements of the dots on the free edge with time while the membrane dried out from fully hydrated to room condition. It can be seen that the free edge of the membrane shrinks and deforms into a meniscus shape as it loses water. Fig. 4 shows the constrained membrane in the frame at the end of the experiment.

A rectangular specimen of a commercial ionomer membrane with three constrained edges and one free edge (on top in the figure) was modeled with ABAQUS. Material curves for 23 °C and hydrations of 25%, 50%, 75% and 100% (underwater tests)

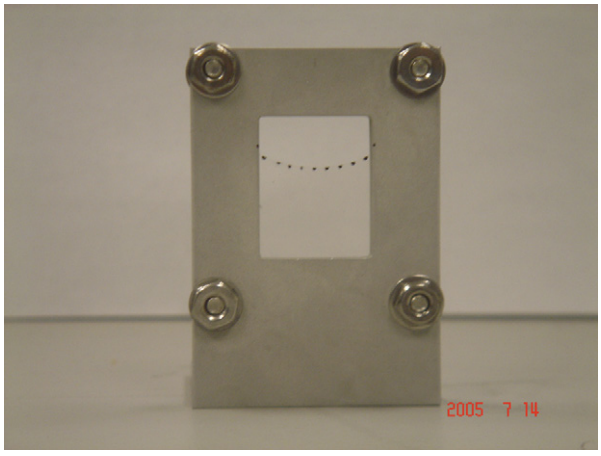

Fig. 4. Clamped membrane in the frame at the end of test.

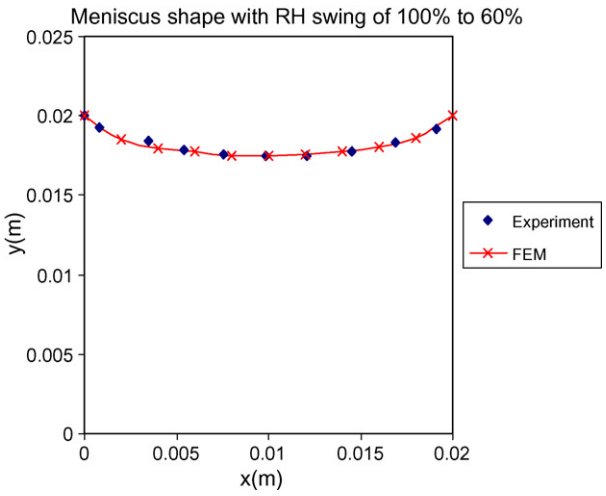

Fig. 5. Comparison of model prediction and experimental measurements.

were incorporated into the model. The applied 'load' was the change in hydration, from 100% to 60% in this case, which was chosen based on the initial and final conditions of the membrane in the validation experiment that was conducted. Fig. 5 shows the deformed meniscus from the experiment along with the predictions of the FEM models. As seen in the picture, by using the proper values for hydration expansion coefficient and material properties correct deformation states of the material can be predicted by using the finite element method as discussed above.

5. Simulation results for a constrained membrane subjected to change in hydration and temperature

It is the purpose of the simulations presented in this section to establish the shrink/expansion stresses and their distributions in a framed membrane subjected to changes in hydration and temperature. As mentioned before, in the fuel cell configuration mechanical failure occurs without external mechanical loads applied in the plane of membrane. The only applied mechanical load is the out-of-plane clamping pressure from the bipolar plates. Hence, the only forces developed in in-plane directions are the tensile/compressive forces due to membrane shrinkage/swelling. However, there is always a contribution from the out-of-plane clamping pressure as a form of compressive stress–strain in the plane of membrane. Out-of-plane pressure tries to squeeze the membrane and therefore pushes the membrane towards the clamped walls. Reaction forces from the walls result in some compressive stress in the plane of the membrane which will be ignored in the simulations. Plane stress simulations are performed. Therefore, there is no out-of-plane contribution in the model and resulting stresses are solely due to in-plane swelling/shrinking behavior. Fig. 8 shows the geometry (30 cm × 30 cm square) and boundary conditions of the finite element model. This model consisted of 400 linear plane stress elements (441 nodes) with clamped boundary conditions at the edges. Clamped boundary conditions are not necessarily the seal locations in the fuel cell assembly. The clamped edges could be a result of any applied force out of plane of the membrane that locally constrains parts of the membrane. These locally constrained geometries could be the results of out-of-plane forces from ribs of bi-polar plates over the gas diffusion layer and, therefore, the membrane. Applied loads are changes in water content (λ) and temperature defined as independent field variables. Elasto-plastic material models are incorporated as explained in Section 3. This elasto-plastic model does not consider the time (rate) response of the polymer membrane; a visco-plastic model is needed to capture time dependency of the material response and will be added subsequent to this work. Hence, the model physically corresponds to a relatively fast drying process close to the uniaxial test strain rates. However, the physical uptake or egress of water in Nafion is quite rapid.

Fig. 6 shows the stress results as temperature and hydration changes are applied to the membrane. The authors have reported previously that crazing is one of the mechanisms contributing to failure of the membrane electrode assemblies [28]. Since crazing is initiated by hydrostatic stress [59] it is essential to study the change in this variable as well as in the deviatoric term as a function of temperature and hydration. It has to be mentioned that since all the analyses in this paper are plane stress and hence σ_{33} is assumed to be zero, the results reported in this paper for stresses, especially hydrostatic stress (σ_{ii}) are conservative results and do not capture all of the clamping pressure effects of the bi-polar plates. In the case shown in Fig. 6, the water content is changing from 1 to 9.2 (water content at fully saturated vapor phase for 80 °C temperature calculated from Eq. (6)) while the temperature changes from 25 °C to 80 °C. Stress-free condition is the dry state where temperature equals 25 °C and water content value is 1. This is analogous to the in-plane condition in which the fuel cell starts up from a relatively dry condition at room temperature to a saturated (wet) mode at operating temperature. It is clear that swelling stress is building up in the membrane with increase in water hydration as temperature also goes up. At some point during hydration, the stress relaxes to a lower value. This could be as a result of the lower stiffness material

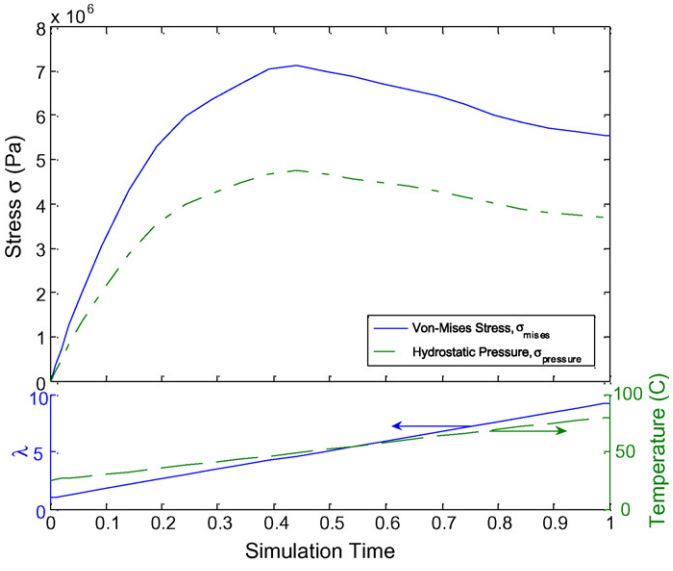

Fig. 6. Von-Mises and hydrostatic stress developed in the membrane as a result of change in hydration (λ: 1 ≥ 9.2) and temperature (*T*: 25 °C ≥ 80 °C).

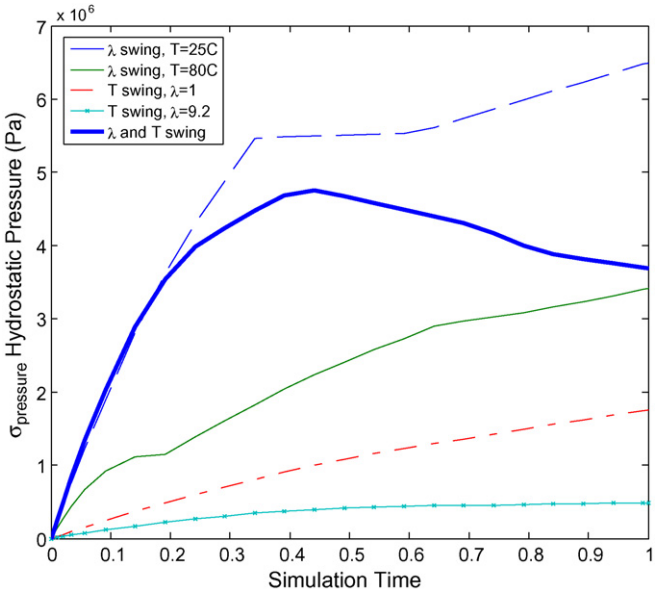

Fig. 7. Hydrostatic stress for different cases of temperature and hydration swing.

properties at higher temperature and moisture as mentioned in Section 2. Basically, smaller stiffness values compensate some of the stress induced by hygro-thermal expansion. Formation of permanent (plastic) deformations due to the increase in hygro-thermal strains also contributes to this relaxation of stress with increases in λ and T.

Obviously, since the membrane is constrained on four sides and there is no non-uniformity in the plane of the membrane, there will not be any resulting in-plane total strain in the model. However, because of the positive values for hygro-thermal strains as a result of expansion tendency of the membrane, there will be negative elastic and plastic strains in the model to maintain zero total strain. Compressive plastic strain during hygro-thermal loadings has been reported in literature [30].

$$\{\varepsilon_{\text{total}}\} = 0 = \{\varepsilon_{\text{elastic}}\} + \{\varepsilon_{\text{plastic}}\} + \{\varepsilon_{\text{hygrothermal}}\} \quad (9)$$

Since the material model at this point does not account for compression, these negative strains will not be further discussed. Fig. 7 compares the simulation results when just temperature or hydration or both are changing. This illustrates the effects of hydration and temperature swings independently in the simulation. In the temperature-only case λ is fixed at 1 and the temperature is changing from 25 °C to 80 °C, while in the hydration-only case, the temperature is fixed at 25 °C and the hydration swing is from 1 to 9.2. It is clear that cycling λ has a far bigger effect than temperature cycles. These results reveal the counter-intuitive nature of the problem when λ, T and material properties change at the same time. From Fig. 7 it can be seen that stress, with just increase in T or λ, is monotonically increasing, but it does not follow the same trend indicated when both T and λ increase simultaneously. This observation points out that simple superposition of each individual case with just increasing T or λ can not be used to get the correct results when both of them increase or decrease at the same time, and it shows the significance of the finite element analysis as a method to obtain the correct behavior.

For all these cases, the simulation results are shown for a node in the middle of the membrane. The simulation results are uniform in the plane of the membrane since there is no non-uniformity in the applied conditions. Generally, in a membrane operating in a fuel cell, point-to-point variations in temperature and hydration of the membrane are inevitable. The membrane tends to be more greatly humidified near the outlet of the flow channels as a result of water production when fuel cell reactions take place.

This non-uniformity dictates different point-wise stress–strain behavior in the membrane during operation. In order to see this effect, a hydration profile is applied across the membrane as shown in Fig. 8. In this case same temperature and hydration change as discussed above was applied, but at the end of these changes hydration was increased near the end of the flow channel (top edge in Fig. 8) from 9.2 to 20 to simulate the possibility of the liquid phase water increasing at the outlet. Stress-free condition is again T = 25 °C and λ = 1. Figs. 9 and 10 show the stress and strain contours of the membrane as a result of this hydration profile. The maximum values for total strain are near the more hydrated edge of the membrane. The strain developed in the plane of the membrane in the constrained configuration could raise wrinkling issues in the membrane near the edges during fuel cell operation. Since material cannot expand in the plane of the membrane, it is possible that it would wrinkle out of its plane due to hydration expansion. Unlike the uniform case where no shear effect was observed, non-uniform hydration also develops shear stress (as well as shear strains) with maximum

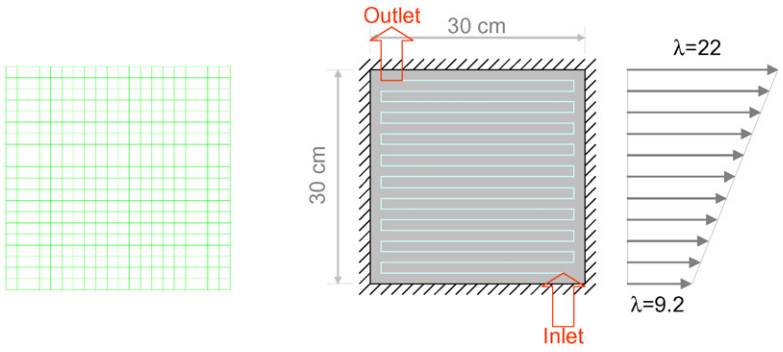

Fig. 8. Generated mesh and schematic of the applied hydration profile as a result of water generation towards the outlet of flow channels.

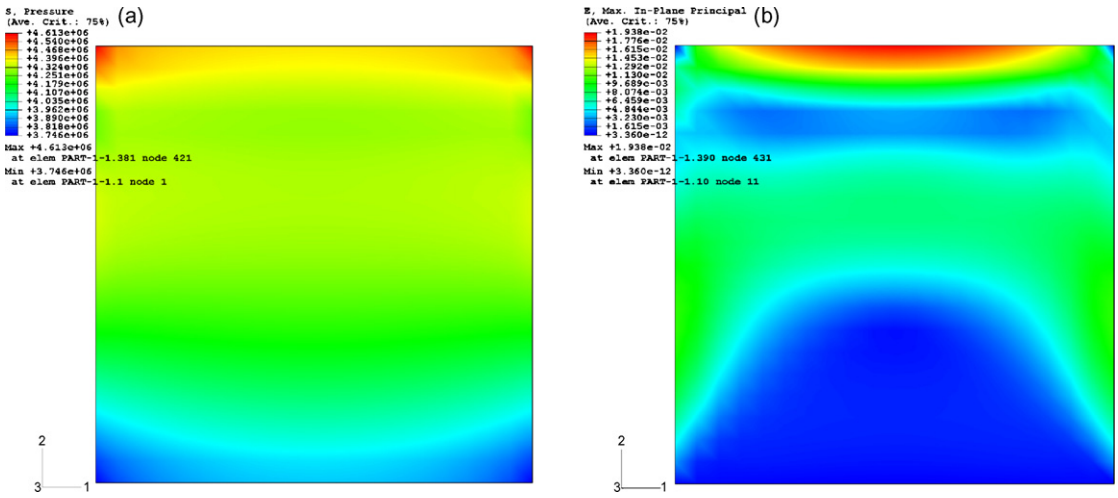

Fig. 9. Contour plot of hydrostatic stress (a) and maximum in-plane principal strain (b) when a linear hydration profile is applied across the membrane. Maximum value for hydrostatic stress is 4.613 MPa near the corners and maximum principal strain is 0.19 around the middle of top edge.

values near the left and right edges (Fig. 10). This observed shear would not be expected for a uniform symmetric geometry. Maximum values of hydrostatic stress happen near the top corners and can be considered as potential spots for failure initiation (Fig. 10a). These results clearly show the significance of the non-uniformities across the membrane, which have to be considered for further understanding of the membrane's mechanical behavior and potential failure modes.

Creation of a hole in the membrane can possibly be considered as the extreme form of non-uniformity in this constraint configuration. A hole in the membrane can represent pinhole creation or even material degradation during fuel cell operation. As part of this modeling work a membrane with a circular hole in the center has been modeled and stress–strain results are studied as a function of change in environmental variables. Geometry is again 30 cm × 30 cm square but this time with a 1.5 cm diameter hole in the center and boundary conditions are again clamped around the edges. Generated mesh has 3608 nodes and 3504 plane stress elements with finer mesh near the hole to capture stress–strain concentrations. Fig. 11 shows the geometry, mesh, and boundary conditions applied to the membrane.

Two different cases will be studied for the center-hole configuration. Firstly, we will consider the uniform change from the stress-free state at $T = 25\,^{\circ}\mathrm{C}$ and $\lambda = 1$ to $T = 80\,^{\circ}\mathrm{C}$ and $\lambda = 9.2$ as it was done before. In the second case, after the first step (modeled in the first case), environmental conditions change in the second step from the previous hot, hydrated state ($T = 80\,^{\circ}\mathrm{C}$ and $\lambda = 9.2$) to the initial cold and dry state which was $T = 25\,^{\circ}\mathrm{C}$ and $\lambda = 1$. These conditions simulate the start-up and shut-down of an operating fuel cell. In the second step the material shrinks while in the first step the material tends to expand. These two steps are repeated five times (equivalent to 10 total start-up and shut-down cycles). This process estimates the accumulative plastic strain developed in each step which can be studied.

Fig. 12 shows the distribution of stress and strain in the membrane with the center hole. From Fig. 12, it can be seen that the stress concentrations are 1.38 for Mises stress and 0.7 for hydrostatic stress component. It should be noted that in the elastic case

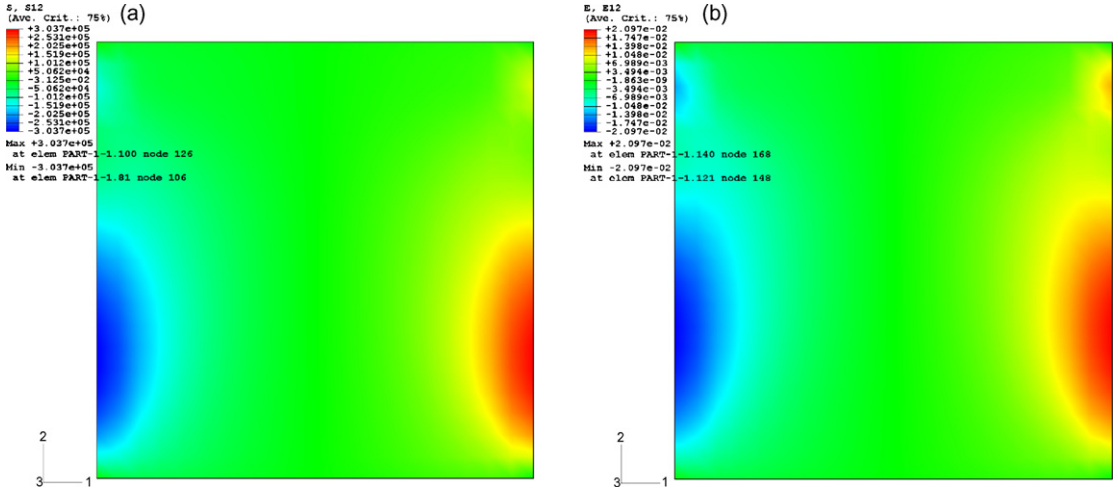

Fig. 10. Contour of shear stress (a) and shear strain (b) developed as a result of non-uniformity in moisture distribution across the plane of membrane. Maximum value for shear stress is 0.3 MPa and for shear strain is 0.02 both near the middle of side edges.

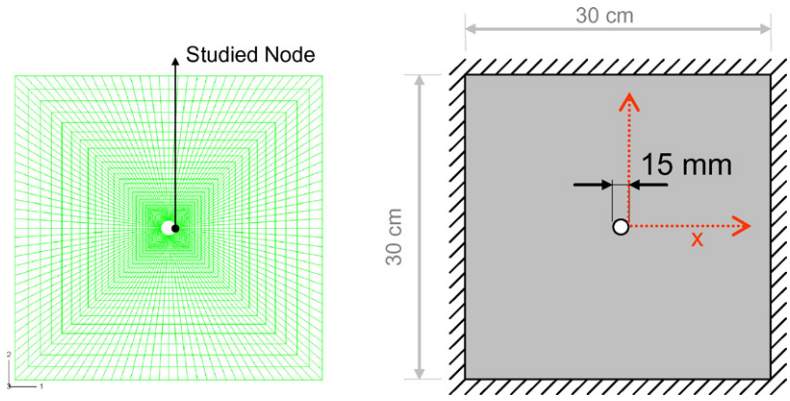

Fig. 11. Geometry and mesh of the constrained membrane with a center hole.

the Mises stress concentration would be 2 and there would be no variation in hydrostatic stress. This can be easily obtained from the elasticity solutions of a biaxially loaded plate. Fig. 12b shows the distribution of maximum principal strains along the centerline of the membrane. As mentioned before, the farfield values for plastic and elastic strains are negative because of the constant positive value for hygro-thermal strain and the constrained geometry (Eq. (9)).

Stress and strain (maximum principal) values at a single node at the edge of the hole (as indicated in Fig. 11) for 10 loading and unloading cycles are shown in Fig. 13. During the unloading cycle (shut down), while the membrane expansion in the loading cycle is shrinking back to the initial dry state, von-Mises stress reaches a minimum value and then at some point increases to a maximum value at the end of the cycle. This maximum value is relatively high and can exceed the ultimate stress values for Nafion® (the maximum von-Mises stress is about 22 MPa in this simulation). Ultimate stress and strain-to-failure values will be reported and discussed further in authors' other publications. This unsymmetrical behavior in loading and unloading is because of the nature of unrecoverable strains developed in the loading cycle. Similar asymmetry is observed in hydrostatic stress.

The most interesting observation is in the plastic strain results. After the first three load/unload cycles plastic strain at the edge of the hole reaches a constant value and does not fluctuate with changes in hydration and temperature. It suggests that there is a saturation value for plastic strain which occurs after a few cycles. This can be associated with the uniform permanent change in the shape of the circular hole as a result of plastic deformation. It can also be seen that other strain and stress results will show similar fluctuations after the first six cycles (three load/unload) cycles because of the constant plastic strains.

6. Visco-plastic model for membrane

Nafion® as a polymer shows strong time dependency. Fig. 14 shows the uniaxial mechanical response of Nafion® at room condition ($T = 25\,^{\circ}C$ and RH = 50%) for different initial strain rates. In each of these curves the specimen is mounted and equilibrated in the environmental chamber at 25 °C and 50% RH for 1 h before the test is performed. The specimens were pulled with different initial strain rates up to an engineering strain of 0.5 and then the displacement was fixed for 1 h in order to observe the stress relaxation. It is clear from this figure that significant overstress is observed for different strain rates and the stress value

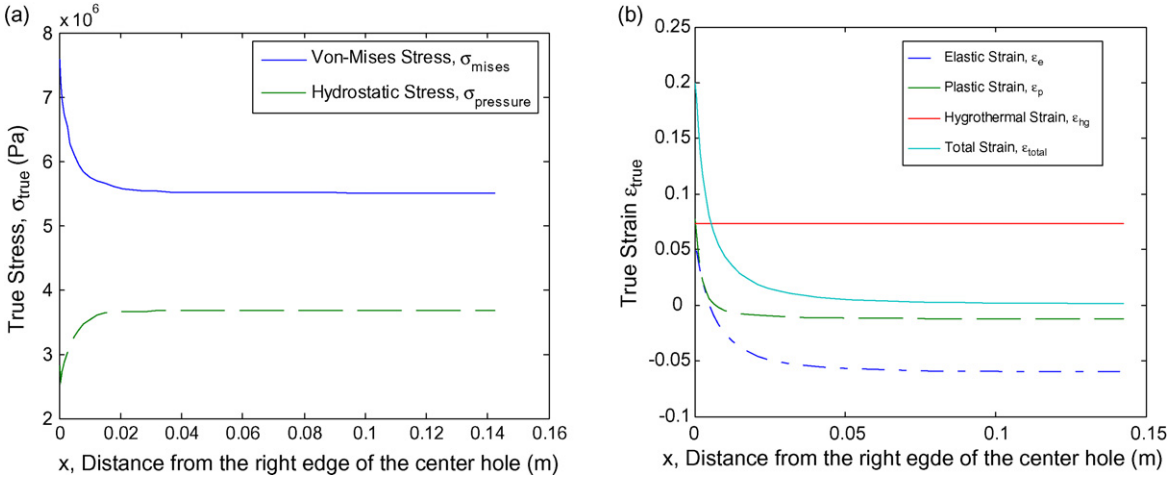

Fig. 12. Stress (a) and strain (b) distribution in the membrane with a hole in the center. *X*-axis shows the distance from the hole in the centerline of the membrane. Strain values are maximum principal strains.

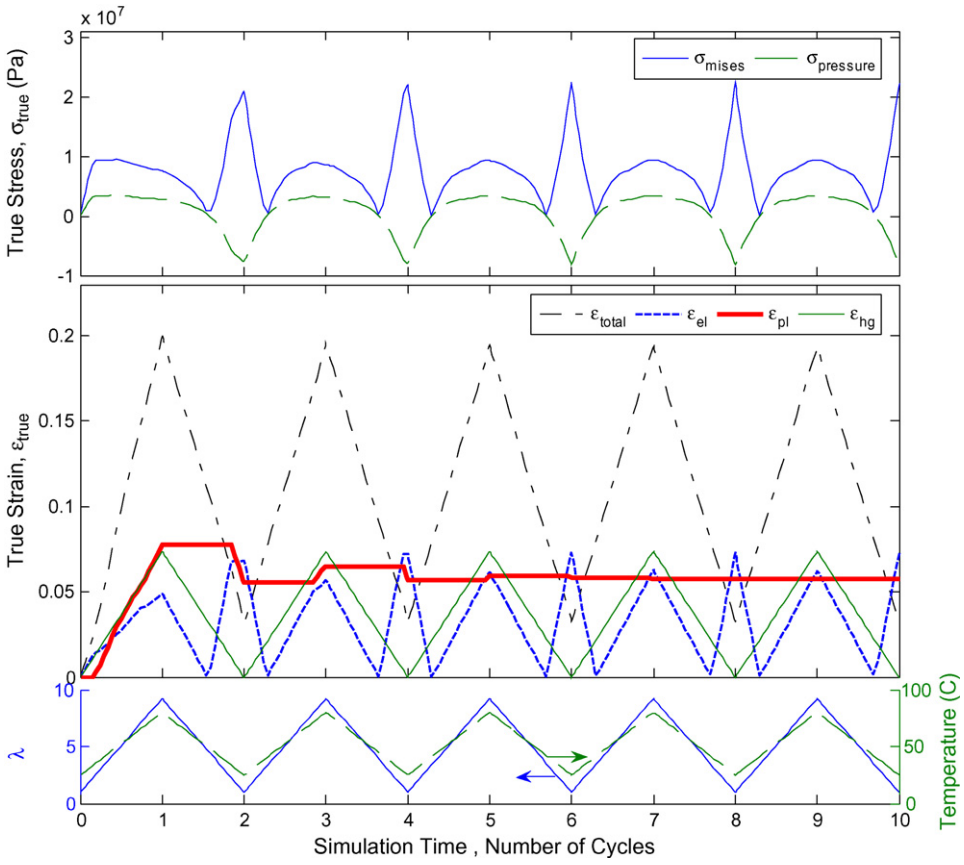

Fig. 13. Stress and strain results at the edge of the hole after ten total load and unload cycles. Plastic strain will be saturated to a constant value after about six cycles. Strain values are maximum principal strains.

relaxes to an equilibrium state with time. Therefore, a classical elasto-plastic model, i.e., classical isotropic plasticity, is not sufficient to capture the accurate stress values when the material exhibits time and rate effects. Stress relaxation for one of the four curves is depicted in Fig. 15.

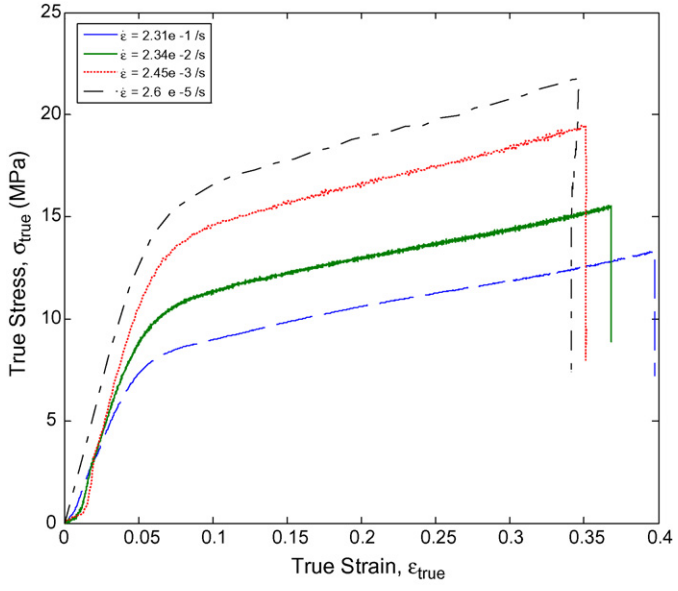

Fig. 14. Stress–strain curves of Nafion® at room conditions for different strain rates.

Previous work reported on Nafion®'s viscous behavior has been reported in the literature in which a linear visco-elastic model, which is accurate in the linear elastic region when applied strains are relatively small, has been used [29]. By assuming visco-elastic behavior for Nafion®, modeling its behavior cannot be accurately done when the material undergoes large strains and is therefore viscoplastic. Because of the large swelling characteristic of membranes in fuel cell/electrolyzer applications, large strains and, therefore, considerable unrecoverable deformations are inevitable.

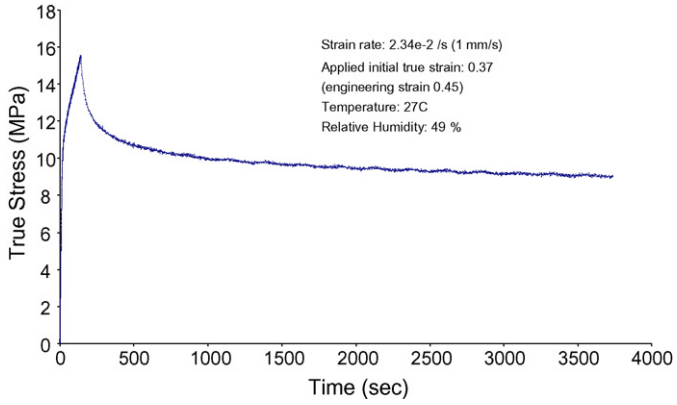

Fig. 15. Stress relaxation of Nafion® at room conditions. Initial applied true strain is 0.37 with strain rate of 2.34e-2.

The authors realize that a more complete viscoplastic model is required to predict stress–strain values for the investigated polymer membranes. In a future paper a two-layer viscoplasticity model will be proposed based on the observed time-dependent behavior of the material and availability of the model in the commercial FEA package ABAQUS (HKS) be used in conjunction with the elastic–plastic module developed in this work. Simulation results based on this model show good agreement with the results shown in Figs. 14 and 15.

7. Conclusion

By incorporating the non-linear material curves for Nafion® NR111 obtained from controlled environment uniaxial experiments in the laboratory and coefficients of hygro-thermal expansion from the literature, an elasto-plastic model was developed and used to estimate the mechanical behavior of Nafion® membrane using the commercial finite element package ABAQUS. A non-linear visco-plastic model is also needed for precise time-dependent modeling of ionomer membranes. However, elasto-plastic simulations still provide valuable insights for understanding the RH-induced straining of the membrane in the constrained fuel cell configurations.

Model simulations show that hydration and drying cycles due to start-up/shut-down of fuel cells can cause significant stresses in the clamped membrane. It is essential to study these induced mechanical stresses to understand the failure of the clamped membrane, where there is no significant external mechanical loads. Hydration is shown to have a bigger effect than temperature in developing mechanical stresses in the membrane. These stresses will be more critical when non-uniformity as a form of hydration profile or a physical pinhole exists across the membrane. As a result of a hydration profile (due to water production in the flow channels), non-uniform stress and strain results were observed in the plane of the membrane with maximum values near the edges. Because of this non-uniformity, shear is seen in the plane of the membrane even though for a symmetric uniform geometry shear effects are usually not expected.

Values for stress and strain concentrations have been obtained near the circular hole formed in the membrane when subjected to changes in hydration and temperature. Because of the permanent deformations (plastic strain), concentration values for deviatoric and hydrostatic stresses are lower than the elastic case. However, in the case of a discontinuity (pinhole) in the plane of the membrane, stress values can exceed the ultimate stress of the material and it is likely that a crack initiates at the edge of the pinhole. By repeating the hydration/dehydration cycles, plastic strain will saturate to a constant value and does not fluctuate after about three load/unloading (six total) cycles in the present case.

Stress–strain results of the constraint configuration due to hydration/dehydration discussed in this paper provide insights to better understand the behavior of ionomer membranes that are clamped and hydrated in fuel cells. These results show the importance of hydration swelling and shrinkage when a new polymer membrane is designed. It is crucial to design and control the expansion properties of a membrane in addition to its electro-chemical properties in the manufacturing process. By reducing the hygro-thermal dimensional change of a membrane, mechanical stress/strains can be reduced which can extend the life of the membrane. Studying in-plane mechanical response of membrane as well as through-the-thickness stress–strain behavior and failure analysis of membranes in the membrane electrode assembly due to mechanical cycling is essential to investigate mechanical degradation of membranes in fuel cells. Detecting the driving forces for mechanical degradation and also chemical degradation of the membrane is necessary to determine the relevant failure modes of such membranes. Mechanistic based failure metrics based on experimental and numerical observations and the present modeling approach will be used in the authors' future work for damage accumulation analysis in durability modeling and life prediction of fuel cells.

Acknowledgements

The work reported here was supported by UTC Power under a cooperative agreement. Technical staff from UTRC assisted in the fabrication of the environment chamber used in this study.

References

[1] The United States Department of Energy (DOE), Hydrogen MYRD&D Plan, 2006.
[2] K.A. Mauritz, R.B. Moore, Chem. Rev. 104 (10) (2004) 4535–4585.
[3] G. Gebel, P. Aldebert, M. Pineri, Polymer 34 (2) (1993) 333–339.
[4] G. Gebel, Polymer 41 (15) (2000) 5829–5838.
[5] A. Eisenberg, Macromolecules 3 (2) (1970) 147–154.
[6] H.-G. Haubold, T. Vad, et al., Electrochim. Acta 46 (10–11) (2001) 1559–1563.
[7] P.J. James, J.A. Elliott, et al., J. Mater. Sci. 35 (20) (2000) 5111–5119.
[8] P.J. James, T.J. McMaster, et al., Polymer 41 (11) (2000) 4223–4231.
[9] M.-H. Kim, C.J. Glinka, et al., Macromolecules 39 (14) (2006) 4775–4787.
[10] J.Y. Li, S. Nemat-Nasser, Mech. Mater. 32 (5) (2000) 303–314.
[11] A.-L. Rollet, O. Diat, G. Gebel, J. Phys. Chem. B 106 (12) (2002) 3033–3036.
[12] L. Rubatat, G. Gebel, O. Diat, Macromolecules 37 (20) (2004) 7772–7783.
[13] T.D. Gierke, G.E. Munn, F.C. Wilson, J. Polym. Sci. Part A-2: Polym. Phys. 19 (11) (1981) 1687–1704.
[14] S.C. Yeo, A. Eisenberg, J. Appl. Polym. Sci. 21 (4) (1977) 875–898.
[15] D. Liu, S. Kyriakides, et al., J. Polym. Sci. Part B: Polym. Phys. 44 (10) (2006) 1453–1465.
[16] T.A.J. Zawodzinski, M. Neeman, et al., J. Phys. Chem. 95 (15) (1991) 6040.
[17] T.A. Zawodzinski Jr., T.E. Springer, et al., J. Electrochem. Soc. 140 (7) (1993) 1981–1985.
[18] J.T. Hinatsu, M. Mizuhata, H. Takenaka, J. Electrochem. Soc. 141 (6) (1994) 1493–1498.
[19] D.R. Morris, X. Sun, J. Appl. Polym. Sci. 50 (8) (1993) 1445–1452.
[20] S.D.F. Bauer, M. Willert-Porada, J. Polym. Sci. Part B: Polym. Phys. 43 (7) (2005) 786–795.
[21] R. Solasi, X. Huang, et al., Proceedings of the 4th International Conference on Fuel Cell Science, Engineering, and Technology 2006, Irvine, CA, 2006.
[22] S. Kundu, L.C. Simon, et al., Polymer 46 (25) (2005) 11707–11715.
[23] Y. Tang, A.M. Karlsson, et al., Mater. Sci. Eng. A 425 (1–2) (2006) 297–304.
[24] M.B. Satterfield, P.W. Majsztrik, et al., J. Polym. Sci. Part B: Polym. Phys. 44 (16) (2006) 2327–2345.
[25] M. Yandrasits, 2nd International Conference on Polymer Batteries and Fuel Cells, Las Vegas, Nevada, 2005.
[26] K. Reifsnider, X. Huang, et al., Rubber Chem. Technol. 79 (5) (2006) 881–891.

[27] W. Liu, K. Ruth, G. Rusch, J. New Mater. Electrochem. Syst. 4 (4) (2001) 227–232.
[28] X. Huang, R. Solasi, et al., J. Polym. Sci. Part B: Polym. Phys. 44 (16) (2006) 2346–2357.
[29] Y.-H. Lai, C.S. Gittleman, et al., Proceedings of the 3rd International Conference on Fuel Cell Science, Engineering, and Technology 2005, Ypsilanti, MI, 2005.
[30] A. Kusoglu, A.M. Karlsson, et al., J. Power Sources 161 (2) (2006) 987–996.
[31] Y. Tang, M.H. Santare, et al., J. Fuel Cell Sci. Technol. 3 (2) (2006) 119–124.
[32] V. Stanic, M. Hoberecht, 4th International Symposium on Proton Conducting Membrane Fuel Cells, Honolulu, Hawaii, 2004.
[33] F. Porchet, P. Javet, Electrochim. Acta 40 (16) (1995) 2569–2577.
[34] M. Inaba, T. Kinumoto, et al., Electrochim. Acta 51 (26) (2006) 5746–5753.
[35] V.O. Mittal, H. Russell Kunz, J.M. Fenton, Electrochem. Solid-State Lett. 9 (6) (2006).
[36] L. Zhang, S. Mukerjee, J. Electrochem. Soc. 153 (6) (2006).
[37] T. Kinumoto, M. Inaba, et al., J. Power Sources 158 (2) (2006) 1222–1228 (Special issue).
[38] J. Qiao, M. Saito, et al., J. Electrochem. Soc. 153 (6) (2006).
[39] W. Liu, D. Zuckerbrod, J. Electrochem. Soc. 152 (6) (2005).
[40] A. Panchenko, H. Dilger, et al., J. Power Sources 127 (1–2) (2004) 325–330.
[41] A. Collier, H. Wang, et al., Int. J. Hydrogen Energy 31 (13) (2006) 1838–1854.
[42] J. Healy, C. Hayden, et al., Fuel Cells 5 (2) (2005) 302–308.
[43] G. Hubner, E. Roduner, J. Mater. Chem. 9 (2) (1999) 409–418.
[44] A.Z. Weber, J. Newman, AIChE J. 50 (12) (2004) 3215–3226.
[45] Y. Tang, M.H. Santare, et al., Proceedings of the 3rd International Conference on Fuel Cell Science, Engineering, and Technology, 2005, Ypsilanti, MI, 2005.
[46] T. Kyu, A. Eisenberg, Journal of Polymer Science, Polymer Symposia, Waco, TX, USA, 1984.
[47] J. Benziger, E. Chia, et al., Chem. Eng. Sci. 60 (6) (2005) 1743–1759.
[48] C. Ishiyama, Y. Higo, J. Polym. Sci. Part B: Polym. Phys. 40 (5) (2002) 460–465.
[49] R.F. Gibson, Principles of Composite Material Mechanics, McGraw-Hill, 1994.
[50] ABAQUS Analysis User's Manual, V 6.5, HKS, 2005.
[51] T.E. Springer, T.A. Zawodzinski, S. Gottesfeld, J. Electrochem. Soc. 138 (8) (1991) 2334–2342.
[52] P.C. Rieke, N.E. Vanderborgh, J. Membr. Sci. 32 (2–3) (1987) 313–328.
[53] K. Broka, P. Ekdunge, J. Appl. Electrochem. 27 (2) (1997) 117–124.
[54] A.Z. Weber, J. Newman, J. Electrochem. Soc. 151 (2) (2004).
[55] N.H. Jalani, R. Datta, J. Membr. Sci. 264 (1–2) (2005) 167–175.
[56] N.H. Jalani, P. Choi, R. Datta, J. Membr. Sci. 254 (1–2) (2005) 31–38.
[57] Physical Properties for Nafion Membrane – Types NR and NRE, E.I. du Pont de Nemours and Company, 2003.
[58] P. Choi, R. Datta, J. Electrochem. Soc. 150 (12) (2003).
[59] B.P. Gearing, L. Anand, Int. J. Solids Struct. 41 (11–12) (2004) 3125–3150.